Commensurate versus incommensurate heterostructures of group-III monochalcogenides

Altaf Ur Rahman,[1,2,*] Juliana M. Morbec,[1,†] Gul Rahman,[2,‡] and Peter Kratzer[1,3,§]
[1]*Faculty of Physics, University of Duisburg-Essen, Lotharstrasse 1, 47057 Duisburg, Germany*
[2]*Department of Physics, Quaid-i-Azam University, Islamabad 45320, Pakistan*
[3]*Center for Nanointegration (CENIDE), University of Duisburg-Essen, Lotharstrasse 1, 47057 Duisburg, Germany*

(Received 24 April 2018; revised manuscript received 11 July 2018; published 4 September 2018)

First-principles calculations based on density-functional theory were performed to investigate heterostructures of group-III monochalcogenides (GaS, GaSe, InS, and InSe) and the effects of incommensurability on their electronic structures. We considered two heterostructures: GaS/GaSe, which has a lattice mismatch of 4.7%, and GaSe/InS, with a smaller mismatch of 2.1%. We computed the cost of having commensurate structures, and we also examined the potential energy landscape of both heterostructures in order to simulate the realistic situation of incommensurate systems. We found that a commensurate heterostructure may be realized in GaSe/InS as the interaction energy of this system with the monolayers assuming the average lattice constant is smaller than the interaction energy of an incommensurate system in which each layer keeps its own lattice constant. For GaS/GaSe, on the other hand, we found that the incommensurate heterostructure is energetically more favorable than the commensurate one, even when taking into account the energetic cost due to the lack of proper registry between the layers. Since the commensurate condition requires that one (or both) layer(s) is (are) strained, we systematically investigated the effect of strain on the band gaps and band-edge positions of the monolayer systems. We found that, in all monolayers, the conduction-band minimum is more than two times more sensitive to applied strain than the valence-band maximum; this was observed to strongly affect the band alignment of GaS/GaSe, as it can change from type-I to type-II with a small variation in the lattice constant of GaS. The GaSe/InS heterostructure was found to have a type-II alignment, which is robust with respect to strain in the range of -2% to $+2\%$.

DOI: 10.1103/PhysRevMaterials.2.094002

I. INTRODUCTION

Successful exfoliation of two-dimensional (2D) materials has boosted interest in such systems for the development of the next generation of nanodevices. In particular, metal monochalcogenides (MMCs) derived from the group-III elements (e.g., GaS, GaSe, InS, and InSe) have been attracting increasing attention due to their excellent optical and electronic properties and their potential for numerous applications. For example, a few layers of GaSe and InSe have been used to build high-performance photodetectors (with fast response, high responsivity, and high external quantum efficiency) [1,2] and highly sensitive phototransistors (with high photoresponsivity and detectivity) [3,4].

In these MMCs, the trivalent metals (Ga and In) form a covalently bonded honeycomb lattice with the hexavalent chalcogen atoms (S and Se). This unusual match of valency that, at first glance, violates the octet rule is made possible by the presence of Ga–Ga or In–In bonds formed between *two* hexagonal networks (see Fig. S1 in the supplemental material [5]). By occupying the bonding orbital of the metal dimer, an extra electron pair (in excess of the octet rule) can be accommodated. The resulting two-dimensional (2D) systems, comprised of two chalcogen and two metal layers, are wide-gap semiconductors [6,7]. Apart from the orbitals contributing to bonding, each chalcogen atom carries a lone pair in an sp-orbital pointing perpendicular to the 2D basal plane [8].

In nature, the MMCs form layered 3D solids formed by stacking of 2D units [9]. Since the lone pairs at chalcogen atoms in adjacent layers of the stack repel each other, such a 3D solid must be held together by dispersion forces (van der Waals interactions between the closed-shell systems formed by each 2D subunit).

The relative position and the magnitude of the band dispersion differ in 3D and 2D structures, and depend on the number of layers in 2D stacks [9–11]. For InSe, in particular, while the 2D single layer has an almost direct band gap between the valence-band maximum (VBM) on a ring circling Γ and the conduction-band minimum (CBM) at Γ, the 3D material in the so-called ε stacking has a direct band gap with both the VBM and CBM directly at Γ [9]. Also, in GaS and GaSe, the top of the valence band around the Γ point is much less dispersive in bulk than in the monolayer counterparts [9]. This variability of the band structure points to the fact that the interaction in stacks of 2D subunits is not solely van der Waals–like, but extended wave functions (over several layers in the stack) exist that lead to shifts of the band edges depending on the stack thickness [12]. In addition, the lateral lattice constant in stacked MMCs may also vary with the number of layers [10], and the sensitivity of the band edges, in particular of the CBM, to change in the lattice constant may contribute to the altered alignment of different bands in the 2D and 3D case. This

*altafqau1@gmail.com
†jmmorbec@gmail.com
‡gulrahman@qau.edu.pk
§peter.kratzer@uni-due.de

situation becomes even more complicated in heterostructures, since both the strain and the different chemical identity of the two parent materials will offset the band structure.

For these reasons, multilayers and heterostructures of MMCs are interesting objects of study. In this paper, we address how the valence and conduction bands of group-III monochalcogenides (GaS, GaSe, InS, and InSe) are affected by stacking in homobilayers and heterostructures; we consider two heterostructures, GaS/GaSe and GaSe/InS, which have lattice mismatches of ∼4.7% and 2.1%, respectively. Experimentally, it must be considered an open question how this mismatch is accommodated in the heterostructure. For example, an experimental work by Woods *et al.* [13] reported that a heterostructure of graphene on top of hexagonal boron nitride undergoes a commensurate-incommensurate transition depending on the rotation angle between the lattices of the two crystals; this experimental observation indicates that it is not always realistic to assume a common lattice constant for the layers in a heterostructure. Because of the periodic boundary conditions enforced in most density-functional-theory codes, first-principles simulations of heterostructures composed of 2D materials with different lattice constants usually employ the following procedures: either (i) a large supercell is used to reduce spurious strain in the individual monolayers, or (ii) one (or both) monolayer(s) is (are) strained to a common lattice constant in a small supercell. Procedure (i) is in many cases computationally too expensive due to the large number of atoms in the simulation. Procedure (ii), on the other hand, may not be realistic since the weak van der Waals interaction between the constituent layers may not be sufficient to strain them during the formation of the heterostructure.

Here we adopt an alternative approach by considering a small (1×1) cell and examining the role of commensurability and incommensurability in the electronic structures of the heterostructures. In the present context of a lattice mismatch of a few percent, we use the term "commensurate" to refer to heterostructures in which the constituent monolayers have a common lattice constant (which means that one or both monolayers are strained) and "incommensurate" for heterostructures in which the monolayers keep their own lattice constant and are not strained. In the commensurate case, the effect of strain, which is required to bring the layers to a common lattice constant, is examined; in the incommensurate case, we explore the potential energy landscape of a series of configurations with different stacking in order to take into account the lack of proper registry between the layers. We additionally compute the costs of having commensurate and incommensurate structures for both GaS/GaSe and GaSe/InS heterostructures in order to predict the most favorable configuration in each case; our results indicate that a commensurate heterostructure may be realized in GaSe/InS while an incommensurate structure is expected for GaS/GaSe. Finally, we estimate the band alignment of the GaS/GaSe and GaSe/InS heterostructures considering both commensurate and incommensurate configurations for each heterostructure.

II. COMPUTATIONAL DETAILS

First-principles calculations within the framework of the density-functional theory (DFT) [14] were performed using the QUANTUM ESPRESSO code [15]. We employed the generalized gradient approximation (GGA) proposed by Perdew, Burke, and Ernzerhof (PBE) [16] for the exchange-correlation functional, the Tkatchenko-Scheffler approach [17] to treat the van der Waals interactions, and norm-conserving Troullier-Martins pseudopotentials [18] to describe the electron-ion interactions (the Ga $3d$ and In $4d$ states were treated as part of the valence shell). The electronic wave functions were expanded in a plane-wave basis set with an energy cutoff of 80 Ry. The Brillouin zone was sampled according to the Monkhorst-Pack method [19] using a $20 \times 20 \times 1$ mesh for the geometry optimization and a denser mesh, $27 \times 27 \times 1$, for the calculations of the electronic structure. Monolayers, bilayers, and heterostructures of GaS, GaSe, InS, and InSe were simulated using the supercell approach with a (1×1) planar unit cell (see Fig. S1 in the supplemental material) and a vacuum region of ∼11 Å along the direction perpendicular to the plane of the layer; a dipole correction as proposed by Bengtsson [20] was employed in the heterostructure systems. For geometry optimizations, all the internal coordinates were allowed to relax until the Hellmann-Feynman forces were smaller than 10^{-3} Ry/bohr. The structural parameters for the monolayer systems computed in this work are in close agreement with first-principles results (computed using different van der Waals methods) previously reported in the literature and with all-electron calculations performed in this work (see Table S1 in the supplemental material).

III. RESULTS AND DISCUSSION

A. Monolayer GaS, GaSe, InS, and InSe

We initially investigated the dependence of the band structure of monolayer GaS, GaSe, InS, and InSe on applied strain. We considered biaxial strain in the range of −15% to 15%, which was simulated by altering the lattice constant a, with strength defined as $\varepsilon = \frac{a-a_0}{a_0} \times 100\%$, where a_0 is the equilibrium lattice constant.

The band structure of the MMCs displays two classes of valence bands: highly dispersive bands due to σ-bonding of metal and chalcogen atoms within the basal plane, and less dispersive bands due to the π-interaction of the lone pairs at the chalcogens. In a single-layer 2D structure, the VBM originates from these π bands. The loci of the maxima are slightly displaced from the Γ point (as shown in Fig. 1, $\varepsilon = 0\%$) and located on a ring (with Γ at its center) in the 2D Brillouin zone [21]. The conduction band has a complex structure as well. A highly dispersive band leads to a minimum at the Γ point [9]; in addition, there are bands dispersing downward and giving rise to a local minimum at the M point.

The unstrained systems were found to exhibit quasidirect band gaps, with the CBM located at the Γ point and the VBM in a ring circling Γ (see Fig. 1, $\varepsilon = 0\%$). We found that the difference between direct and indirect band gaps is smaller than 0.1 eV for all monolayers; the calculated indirect/direct band gaps for monolayer GaS, GaSe, InS, and InSe are 2.24/2.33, 1.81/1.90, 1.72/1.80, and 1.55/1.62 eV, respectively, which are in good agreement with values obtained in previous DFT-PBE calculations [7,9,22,23]. We notice that there is a large scattering in the values for the band gaps reported in the literature

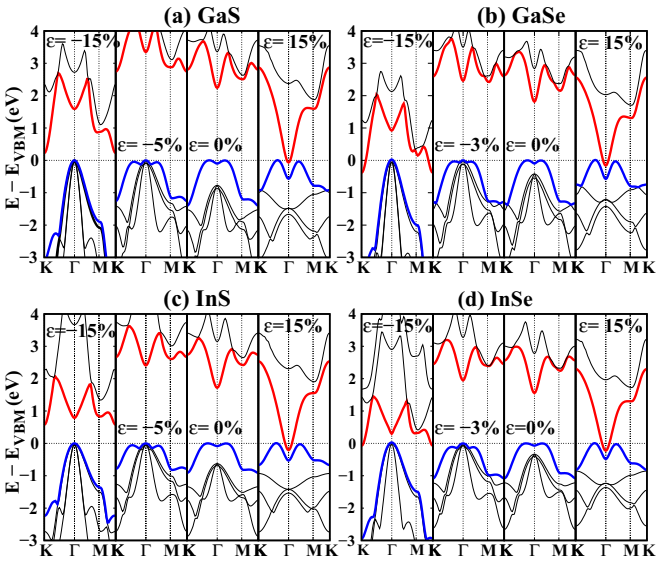

FIG. 1. Computed band structures of monolayer (a) GaS, (b) GaSe, (c) InS, and (d) InSe for different values of strain ε. Red and blue lines indicate the lowest conduction band and the highest valence band, respectively. The zero energy is set at the VBM.

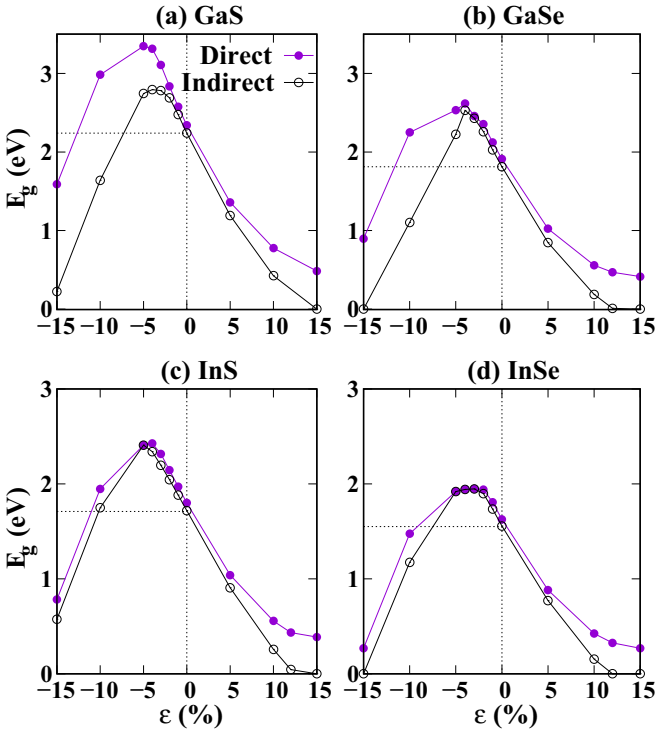

FIG. 2. Computed direct and indirect band gaps, E_g, as a function of strain, ε, for monolayer (a) GaS, (b) GaSe, (c) InS, and (d) InSe. Filled magenta and open black circles correspond to direct and indirect band gaps, respectively. The dashed lines indicate the smallest band gap at equilibrium lattice constant.

(for example, the band gap of monolayer GaSe obtained using PBE exchange-correlation functional varies from 1.77 [22] to 2.21 eV [24]) and we believe this is due to the different lattice constants obtained with different pseudopotentials (the lattice constants of monolayer GaSe in the aforementioned studies were 3.82 and 3.75 Å, respectively); in fact, as we will discuss in the next paragraphs, the band gaps of monolayer GaS, GaSe, InS, and InSe are very sensitive to strain, and a small decrease of 2% in the lattice constant can lead to an increase of up to 23% in the band gap.

We found that tensile strain leads to a reduction in the band gap of all monolayers—consistent with results reported in Refs. [7,10,24–27], which were obtained using either PBE or HSE06 exchange-correlation functionals with the vdw-optB88 or the DFT-D2 van der Waals methods—with a semiconductor-to-metal transition occurring at strain between 10% and 15% (see Fig. 2). Interestingly, we observe that the dependence of the band gap on tensile strain seems to be stronger in the selenides than in the sulfides: while at 5% strain, the band gaps of GaS and InS are reduced by about 47% with respect to the unstrained systems, the reductions for GaSe and InSe are ∼53% and 50%, respectively. As a consequence, the semiconductor-to-metal transition in selenides, which have narrower band gaps at zero strain, is expected to occur at lower strain values (12% strain, according to our DFT-PBE calculations) than in sulfides (which have wider band gaps at zero strain), for which 15% strain is required. Similar findings have been reported earlier from DFT-PBE calculations for GaS and GaSe [24] and for InSe [25]. We would like to point out that the critical strain values for the semiconductor-to-metal transition depend on the band gap of the unstrained system, and they are expected to be higher in GW and HSE calculations, since PBE underestimates the band gap in comparison with GW and HSE band gaps; however, our conclusion concerning the order of the transition (selenides first, then sulfides) is expected to remain valid in the HSE and the GW method, since all methods agree on the relative order of the band gaps in selenides and sulfides [7].

For compressive strain we found that the band gaps increase for small strain values (up to 4% for GaS and GaSe, 5% for InS, and 3% for InSe) and decrease for larger strain (see Fig. 2); our results for InS and InSe are consistent with DFT results reported in Refs. [25] (obtained using the PBE functional) and [26] (obtained using the HSE06 functional and the DFT-D2 vdW method). For small strain values we observe again a stronger strain dependence in the selenide monolayers: for −2%, the band gaps of GaSe and InSe increase by about 25% and 22%, respectively, while the band gaps of GaS and InS increase only by ∼20% and 19%, respectively.

Examining the dependence of the band edges on biaxial strain, as shown in Fig. 1, we found that the CBM at the Γ point is particularly highly sensitive to strain: under tensile strain, it moves downward, and eventually (at a critical tensile strain that our DFT-PBE calculations predicted to be +12% for GaSe and InSe and +15% for GaS and InS) overlaps with the valence band of π-type that moves upward under the tensile strain, leading to a semiconductor-to-metal transition (as discussed above). Most characteristic of (small) compressive strains is a shift of the relative energetic position of the valence bands: the highly dispersive σ band increases its dispersion under compression, its maximum at Γ moves to higher energies, and at some (negative) strain value it "overtakes" the π band (Fig. 1, second panels from the left). Then, the new VBM

TABLE I. Calculated deformation potentials Ξ (in eV) of monolayer GaS, GaSe, InS, and InSe. Ξ_v, Ξ_c, and Ξ_{gap} are the deformation potentials for the VBM, CBM, and band gap, respectively. We used absolute values for the strain tensor; for example, for 2% strain we used $\varepsilon_{xx} = \varepsilon_{yy} = 0.02$.

	GaS	GaSe	InS	InSe
Ξ_c (eV)	−8.51	−8.93	−5.90	−5.88
Ξ_v (eV)	2.22	1.59	2.40	2.34
Ξ_{gap} (eV)	−10.73	−10.52	−8.30	−8.22

is formed by the maximum of the σ band. Such a behavior can be understood by considering the increased overlap of orbitals under compressive strain, which primarily affects the σ bonds. This behavior results in the VBM (due to the σ band) being eventually located at the Γ point, leading to an indirect-to-direct transition in InS (at −5% strain) and InSe (at −3% strain) or to a situation of a quasidirect band gap in GaSe at −3% strain, when the indirect band gap exceeds the direct one by no more than 20 meV (see Fig. 2). At higher compressive strain larger than 5%, further change in the conduction band is observed: the CBM moves away from the Γ point (as shown in Fig. 1 for $\varepsilon = -15\%$), making it hard to realize a direct Γ-Γ transition even if compressively strained layers have their VBM at the Γ point; as a consequence, we observe an increase in the difference between direct and indirect band gaps under compressive strain, in particular for GaS and GaSe [Figs. 2(a) and 2(b)].

For small strain values in the range of −2% to +2%, its effect on the CBM and VBM can be described by the hydrostatic deformation potential Ξ. The band extremum of a band with energy E_i is then given by $E_i + \Xi\,\mathrm{Tr}(\varepsilon)$, where ε is the strain tensor. To determine Ξ, we calculate the band positions in a strained sample relative to the vacuum level in the same calculation. The results are shown in Table I. We notice that the deformation potential of the CBM is more than two times larger than that of the VBM, indicating that the CBM is more sensitive to strain (as we have discussed in the previous paragraphs), especially for the Ga-based systems. From the absolute deformation potentials of the VBM, Ξ_v, and of the CBM, Ξ_c, we can directly obtain the band-gap deformation potential as follows: $\Xi_{gap} = \Xi_c - \Xi_v$. We observe that the strain dependence of the band gap is quite similar in sulfides and selenides, being only slightly stronger in the former (by ∼0.21 eV per strain unit in Ga-based systems and 0.08 eV per strain unit in In-based systems). Therefore, we conclude that monolayer GaS and InS reach zero band gap for larger strain values than their selenide counterparts because of their wider band gaps at 0% strain.

B. Homobilayers

We next briefly examined the change in the band structure due to the formation of homobilayer systems. For simplicity, we considered only the so-called AA stacking, which has a mirror plane between the two layers (i.e., the atoms in the second layer have the same planar coordinates as those in the first layer). Different stackings can also be realized deriving

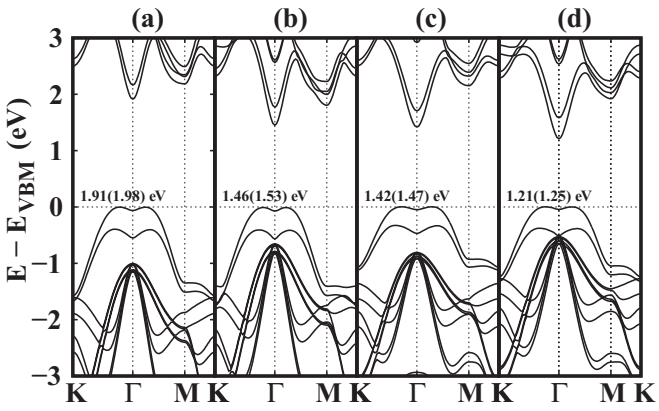

FIG. 3. Band structures of bilayer (a) GaS, (b) GaSe, (c) InS, and (d) InSe. Indirect and direct (in parentheses) band gaps are listed for each system. The zero energy is set at the VBM in all cases.

from the ε and β polytypes (the latter possesses an inversion center) [9].

From the band structure of the homobilayers (see Fig. 3), it is obvious that the bands occur in pairs. Of these pairs of bands, one band has a wave function with positive parity under mirror symmetry, while the second band has negative parity under the corresponding symmetry operation. The energy splitting within these pairs of bands, corresponding to bonding and antibonding linear combinations of the orbitals in each monolayer, results in a narrowing of the band gap. Our computed indirect/direct band gaps for bilayer GaS, GaSe, InS, and InSe are 1.91/1.98, 1.46/1.53, 1.42/1.47, and 1.21/1.25 eV, respectively, which are 0.3–0.4 eV smaller than the values obtained for the monolayer systems; these differences come from a downward shift of the CBM, upon bilayer formation, by values between 0.11 and 0.16 eV and an upward shift of the VBM by values between 0.15 and 0.24 eV. For practical applications, our results suggest, for example, that bilayer GaS and GaSe are more promising for water splitting than the monolayer systems, as the narrowing of the band gaps would lead to a larger absorption of the solar spectrum; as has been pointed out by Zhuang and Hennig in Ref. [7], single-layer GaS and GaSe have too large band gaps. On the other hand, for InS and InSe the formation of bilayers is detrimental for water splitting as the CBM of the monolayers are already too close to the H^+/H_2 redox potential [7], and the downward shift caused by the bilayer formation may bring the CBM below the H^+/H_2 potential. The narrowing of the gaps observed in the homobilayers is consistent with the smaller band gaps of the bulk systems in comparison with the monolayers [9,28]. For InSe, in particular, we observe that the formation of bilayers reduces the difference between direct and indirect band gaps from 0.07 eV in the monolayer system to 0.04 eV in a bilayer, which is consistent with the indirect-to-direct band-gap crossover, as the number of layers is increased, obtained in previous DFT-PBE calculations reported in Refs. [11,28].

Regarding the structural properties, we did not find any significant change in the structural parameters (lattice constant, bond length, layer thickness) upon the formation of bilayers, as can be seen in Table S2 in the supplemental material; a similar finding was reported in a previous DFT-PBE study

for bilayer and trilayer GaS and GaSe [29]. The optimized interlayer distances (distance between the top chalcogen atom of the bottom layer and the bottom chalcogen atom of the top layer) for bilayer GaS, GaSe, InS, and InSe are 3.74, 3.96, 3.79, and 3.93 Å, respectively; the values for GaSe and InSe are ∼0.6 and 0.8 Å larger than previous theoretical (DFT-PBE) interlayer distances computed for ε-type 3D systems [30].

The interaction E_b for the bilayer systems (and for the heterostructures in Sec. III C) can be computed as

$$E_b = E_{M_1C_1/M_2C_2} - E_{M_1C_1} - E_{M_2C_2}, \quad (1)$$

where $E_{M_1C_1/M_2C_2}$ is the total energy of the bilayer (or the heterostructure), $E_{M_1C_1}$ and $E_{M_2C_2}$ are the total energies of the individual layers, M = In,Ga and C = S,Se, and $1 \equiv 2$ in the homobilayer systems. We obtained E_b of −90.6, −93.4, −93.1, and −98.6 meV per (1×1) cell (or −7.9, −7.4, −7.1, and −6.9 meV/Å^2) for bilayer GaS, GaSe, InS, and InSe, respectively. These values are in the range of those computed (using the PBE functional and the DFT-D2 vdW method) in Ref. [31] for bilayer MoS_2, $MoSe_2$, WS_2, and WSe_2 (44.8–125.9 meV per formula unit). The effect of the van der Waals (vdW) interaction in the bilayer systems can be estimated by computing the interaction energies without the vdW correction; we found E_b (PBE only) of −0.6, −3.9, −5.4, and −6.9 meV per (1×1) unit cell for bilayer GaS, GaSe, InS, and InSe, respectively, which is more than one order of magnitude smaller than the interaction energies obtained with vdW correction. The interlayer distances of bilayer GaS, GaSe, InS, and InSe computed without vdW correction were found to be, respectively, 0.42, 0.35, 0.76, and 0.67 Å larger than those obtained with the vdW-TS method.

C. van der Waals heterostructures

1. Commensurate versus incommensurate heterostructures

The van der Waals interaction between the layers in a heterostructure is strongly distance-dependent. The optimum bonding distance between two layers results from the balance between repulsive forces (between the "electron clouds") and attractive van der Waals forces. From this argument, it becomes clear that there is a preferred registry between two layers held together by van der Waals forces. However, perfect registry between *different* materials requires that they take on a common lattice constant. This is possible only if one (or both) layer(s) is (are) strained. Straining the layers comes with an energetic cost that makes the formation of a commensurate structure less favorable the larger the mismatch between their lattice constants. Thus, one may expect that both commensurate and incommensurate heterostructures can exist, depending on the lattice mismatch, the elastic moduli of the layers, as well as on the corrugation depth of the interaction potential between the layers.

Given the sensitivity of the band gap and the band edges in MMCs to strain (as can be seen in Fig. 2 and from the large deformation potentials in Table I), the strain state of a layer in a heterostructure is expected to have a significant impact on the band gap that can be realized by experimentally preparing a certain type of heterostructure. In the following, we address this issues by studying two prototypical examples: (i) the GaS/GaSe heterostructure, which has a considerable lattice mismatch of 4.7%, and (ii) the GaSe/InS heterostructure, whose layers deviate in their lattice constants only by 2.1%, making it a potential candidate for commensurate heterostructure formation.

In the commensurate heterostructure, both layers are assumed to have the same lattice constant, which was chosen taking into consideration the elastic properties of the layers. We computed the elastic modulus C of each monolayer using $C = (\frac{1}{A_0})(\frac{\partial^2 E}{\partial \varepsilon^2})$, as suggested in Refs. [7,26], where A_0 is the equilibrium area of the simulation cell and E is the energy at strain ε. We found C = 109, 94, 86, and 74 N/m for GaS, GaSe, InS, and InSe, respectively, which are in the range of the values reported in previous theoretical work, namely 98 (120), 79 (104), 73 (89), and 60 (76) N/m for GaS, GaSe, InS, and InSe, respectively [7], obtained using the PBE (HSE06) functional, and 86.75 and 70.63 N/m for InS and InSe [26] obtained using the HSE06 functional. Using our computed values for the elastic modulus, we can estimate the optimal common lattice constant $\bar{a}$ that would minimize the strain energy in the heterostructure; we found $\bar{a}$ = 3.721 Å for GaS/GaSe and 3.858 Å for GaSe/InS. Note that the values for $\bar{a}$ are very close to the average lattice constant of the heterostructures, namely 3.73 Å in GaS/GaSe and 3.86 Å in GaSe/InS. From Eq. (1) we can calculate the interaction energy of the commensurate heterostructures; the terms $E_{M_1C_1}$ and $E_{M_2C_2}$ are evaluated at their respective monolayer lattice constant, i.e., in the strain-free state. Due to the attractive van der Waals interaction, we find that the overall interaction is still attractive, despite the energy cost of straining the layers, by −49 meV for GaS/GaSe and −149 meV for GaSe/InS, per (1×1) unit cell, respectively.

In the calculation of E_b for the incommensurate heterostructures, we tentatively consider the larger of the two monolayer lattice constants, i.e., a_{GaSe} for the GaS/GaSe and a_{InS} for the GaSe/InS heterostructure, as the common one. The reference energy of the material with the smaller lattice constant entering Eq. (1) is taken in the strained state. Defined in this way, E_b solely contains the contribution of the attractive van der Waals interaction, which amounts to −155 meV for GaS/GaSe and −164 meV for InS/GaSe, per (1×1) unit cell. This procedure is justified if we consider that in the real, incommensurate structure, each layer of the heterostructure takes on its own lattice constant, and hence strain contributions are absent (apart from small local variations in the lattice constant that could lead to small local strain contributions).

To model the realistic situation of incommensurate heterostructures, we need to take into account that the match between the two atomic layers is by no means perfect, and therefore the interaction estimated by E_b is an upper bound. To get a more realistic estimate, a correction ΔE_{inc} is applied that is obtained as follows: we perform a series of DFT+vdW calculations to explore the corrugated potential energy landscape of van der Waals bonding. In practice, we generated a series of configurations considering different stacking for the metal (M) and chalcogen (C) atoms of each layer. Figure 4 displays the six configurations we considered for both GaS/GaSe and GaSe/InS heterostructures. For example, Fig. 4(a) shows the configuration $M_T/C_B + C_T/M_B$, where the metal atom of the top layer (M_T) is located on top of the chalcogen atom

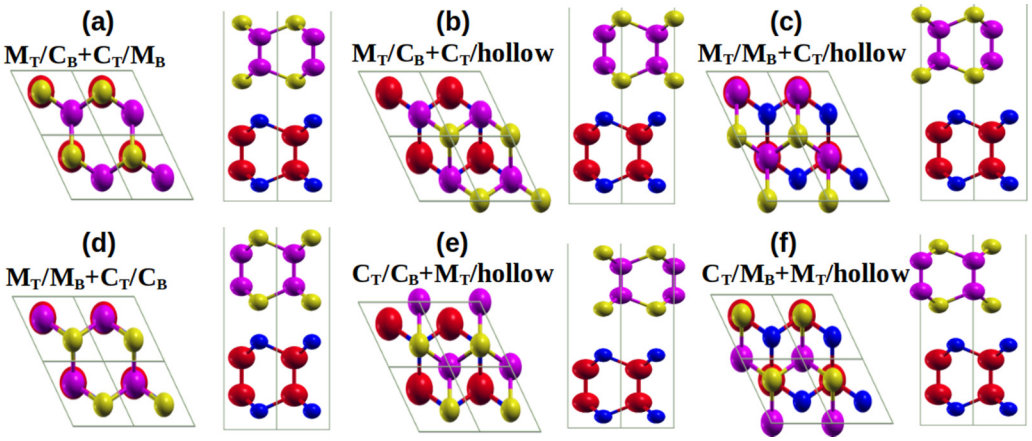

FIG. 4. Schematic top and side views of the different configurations considered here for the GaSe/InS heterostructure. M_T (C_T) and M_B (C_B) refer to metal (chalcogen) atoms of top and bottom layers, respectively. Red, magenta, yellow, and blue balls correspond to In, Ga, Se, and S atoms, respectively. The same configurations were considered for the GaS/GaSe heterostructure.

of the bottom layer (C_B) and the chalcogen atom of the top layer (C_T) sits on top of the metal atom of the bottom layer (M_B), and Fig. 4(b) shows the configuration $M_T/C_B + C_T$/hollow, where the metal atom of the top layer (M_T) is located on top of the chalcogen atom of the bottom layer (C_B) and the chalcogen atom of the top layer (C_T) sits on the hollow site of the bottom layer.

The results for relative energies, interlayer distances (vertical distance between the bottom chalcogen atom of the top layer and the top chalcogen atom of the bottom layer), and band gaps of the six configurations investigated here are displayed in Table II. We notice that in both heterostructures, the stacking of S on Se atoms (configurations d and e) is energetically unfavorable (a similar finding has also been reported for the $MoS_2/MoSe_2$ heterostructure [32]). This can be rationalized if we keep in mind the repulsion between the electrons forming the lone pairs at each chalcogen which point toward each other in this configuration. For the GaS/GaSe heterostructure, the energetically most favorable configuration occurs when both the S atoms and the Se atoms point toward the Ga atoms in the other respective layer (configuration a); this configuration is also realized in the homogeneous stacking in 3D GaS in the β-phase [9]. For the GaSe/InS heterostructure, the energetic minimum is at configuration f, where only the In atoms of the InS layer sit above the Se atoms, while the Ga atoms are located in hollow positions with respect to the InS lattice. The two lattices are rotated with respect to each other, characteristic of an AB stacking. The interlayer distances in both heterostructures depend on the stacking, with the largest distances occurring in the most unfavorable configurations.

Interestingly, the size of the band gap also changes in dependence on the registry between the layers, as can be seen from the rightmost column of Table II; our results show that different stackings can cause variations of up to 10% in the band gaps. It is also interesting that the band gaps of the heterostructures are significantly smaller than the band gaps of the individual monolayers (we will discuss this in more detail in the next paragraphs). Our results for the band gaps are in good agreement with those obtained in previous DFT-PBE studies [23,33].

In an incommensurate heterostructure, one would expect that each of the configurations is realized somewhere since the relative positions of the two layers change from site to site. Forming the average of the interaction energies can be used to estimate the energetic cost of a structure that misses the proper registry between the layers. In GaS/GaSe, this average interaction energy $E_b + \Delta E_{\text{inc}}$ amounts to -125 meV per (1×1) cell or -9.9 meV/Å^2, while in GaSe/InS it is

TABLE II. Relative formation energies ΔE, interlayer distances h_{CC} (vertical distance between the bottom chalcogen atom of the top layer and the top chalcogen atom of the bottom layer), and indirect/direct band gaps E_g^I/E_g^D of the different configurations considered for the GaS/GaSe and GaSe/InS heterostructures (see Fig. 4); for the in-plane dimensions of the simulated supercells, we considered the larger of the two monolayer lattice constants (a_{GaSe} for GaS/GaSe and a_{InS} for GaSe/InS). The most stable configuration in each case was set to zero energy. The average of the relative formation energies, ΔE_{inc}, is given for each heterostructure.

Configuration	ΔE (meV)	h_{CC} (Å)	E_g^I/E_g^D (eV)
GaS/GaSe			
a ($Ga_T/Se_B + S_T/Ga_B$)	0.0	3.27	0.89/0.96
b ($Ga_T/Se_B + S_T$/hollow)	23.8	3.76	0.95/1.02
c ($Ga_T/Ga_B + S_T$/hollow)	24.6	3.67	0.94/1.00
d ($Ga_T/Ga_B + S_T/Se_B$)	58.0	3.92	0.91/0.99
e ($S_T/Se_B + Ga_T$/hollow)	73.8	3.74	0.86/0.95
f ($S_T/Ga_B + Ga_T$/hollow)	1.8	3.26	0.88/0.94
average (ΔE_{inc})	30.3		
GaSe/InS			
a ($Ga_T/S_B + Se_T/In_B$)	7.1	3.23	0.98/1.06
b ($Ga_T/S_B + Se_T$/hollow)	11.2	3.23	0.96/1.05
c ($Ga_T/In_B + Se_T$/hollow)	12.9	3.23	0.96/1.04
d ($Ga_T/In_B + Se_T/S_B$)	72.0	3.92	1.02/1.12
e ($Se_T/S_B + Ga_T$/hollow)	63.8	3.91	1.02/1.12
f ($Se_T/In_B + Ga_T$/hollow)	0.0	3.23	0.97/1.06
average (ΔE_{inc})	27.8		

-136 meV per (1×1) cell or -10.3 meV/Å^2. These values contain the average cost, due to the variation in atomic registry between the layers, of $\Delta E_{\text{inc}} = 30$ meV per (1×1) cell for the GaS/GaSe heterostructure, and $\Delta E_{\text{inc}} = 28$ meV per (1×1) cell for the GaSe/InS heterostructure. The smaller cost for the GaSe/InS heterostructure is consistent with its smaller lattice mismatch. Comparing the interaction energies of the incommensurate and the commensurate (in which the layers assume the average lattice constant of the system) structures for GaSe/InS (~ -136 and -149 meV, respectively), we find that the latter has smaller energy, indicating that a commensurate heterostructure is expected for this system. For GaS/GaSe, on the other hand, the interaction in the incommensurate case (~ -125 meV) is much stronger than that in the commensurate case (-49 meV), suggesting that GaS/GaSe will form a incommensurate heterostructure, with each layer keeping its own lattice constant.

2. Band alignment

By inspecting the projected density of states (PDOS) of the heterostructures, shown in Fig. 5, we observe that in both systems the highest valence bands mainly originate from the p-orbitals of the Se atoms; in the GaS/GaSe heterostructure [Fig. 5(a)] we observe a smaller contribution from the S p orbitals to the VBM, while in the GaSe/InS heterostructure [Fig. 5(b)] the contribution from the S orbitals starts only around 1 eV below the VBM. The composition of the bottom of the conduction band differs in the two heterostructures considered here: in the GaS/GaSe heterostructure, it is formed by a mixture of Ga s, Ga p, and S p orbitals, while in the InS/GaSe heterostructure, it is composed of In s, In p, and S p orbitals.

The analysis of the PDOS of the GaSe/InS heterostructure [Fig. 5(b)] suggests that the VBM and the CBM are located in different layers. In fact, by examining the band alignment [Fig. 6(b)] we found that the VBM is located in the GaSe layer, both in the case where the layer conserves its own lattice constant [3.82 Å, left panel of Fig. 6(b)] and when it is stretched to the largest lattice constant in the heterostructure [3.90 Å, right panel of Fig. 6(b)], while the CBM is located in the InS layer. This indicates that the GaSe/InS heterostructure exhibits a type-II alignment, which is promising for photovoltaic applications; a similar finding has been reported in Refs. [7] (DFT-HSE06) and [23] (DFT-PBE). The type-II band alignment in the GaSe/InS heterostructure is robust with respect to small strain values in the range of -2% to 2%, since the VBM and CBM offsets (0.56 and 0.65 eV, respectively) between the InS and GaSe monolayers are larger than the variation in the band edges caused by strain ($<$0.36 eV for the CBM and $<$ 0.10 eV for the VBM, computed using the deformation potentials listed in Table I).

For the GaS/GaSe heterostructure [Fig. 6(a)] we observe a type-I band alignment—with both VBM and CBM located in the GaSe layer—if both layers conserve their own lattice constants (left panel). However, we notice that the CBM offset between the GaS and GaSe layers is very small (only 0.06 eV), which suggests that the band alignment may be changed to type-II with a small variation (by only 0.36%, computed using the deformation potentials in Table I) in the lattice constant

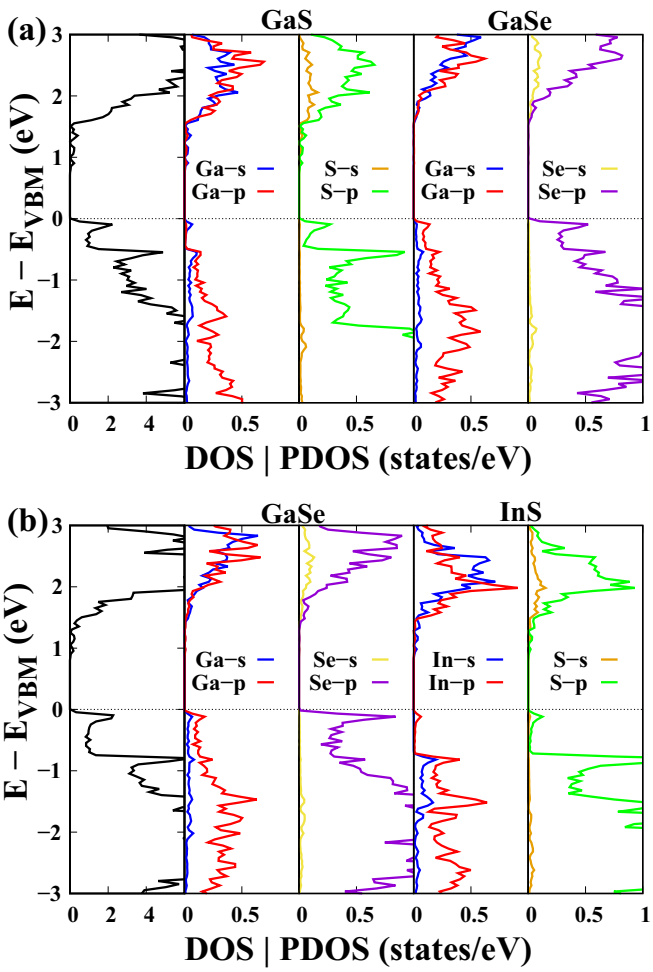

FIG. 5. Projected density of states (PDOS) of the (a) GaS/GaSe and (b) GaSe/InS heterostructures. Here the heterostructures were simulated assuming the largest lattice constant between the constituent layers: a_{GaSe} for GaS/GaSe and a_{InS} for GaSe/InS. The total DOS is shown in the left panel of each figure. The zero energy is set at the VBM.

of GaS; in fact, we observe a type-II alignment if both GaS and GaSe layers have the larger lattice constant of the system (3.82 Å, right panel). The CBM and VBM offsets between GaS and GaSe ($\Delta E^{\text{CBM/VBM}} = E^{\text{CBM/VBM}}_{\text{GaS}} - E^{\text{CBM/VBM}}_{\text{GaSe}}$) obtained here for the case where both layers keep their own lattice constants [left panel in Fig. 6(a)], namely $+0.06$ and -0.37 eV, respectively, are in fair agreement with those computed by Zhuang and Hennig [7] using the GW approximation (-0.06 and -0.54 eV, respectively). While quantitative values for the band offset from PBE should be considered less reliable than the GW results, one can conclude from both methods that the incommensurate GaS/GaSe heterostructure is close to a type-I/type-II transition driven by strain. For GaSe/InS, considering that each layer assumes its own lattice constant [left panel of Fig. 6(b)], we also found a fair agreement between our computed $\Delta E^{\text{CBM/VBM}}$ ($+0.65$ and $+0.54$ eV, respectively) and those computed in Ref. [7] using the GW approximation ($+0.82$ and $+0.64$ eV). Although PBE band gaps are underestimated with respect to those obtained using hybrid functionals or the GW approximation, we expect that

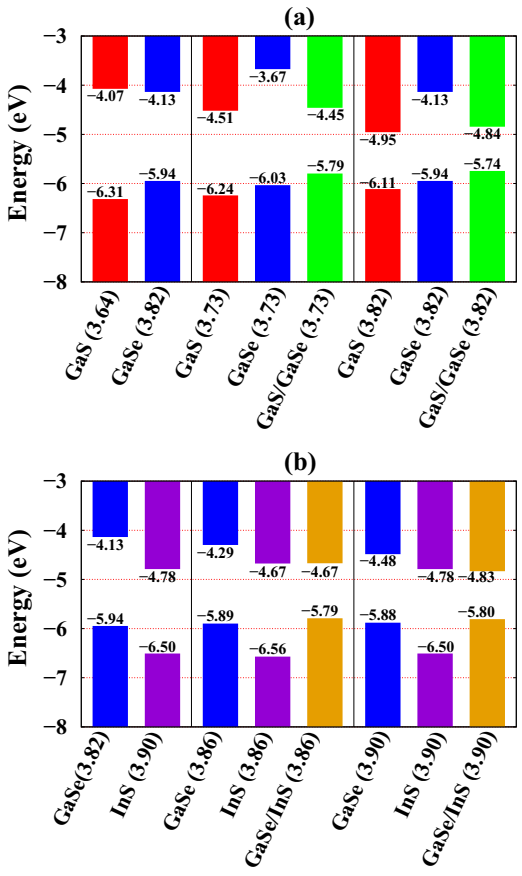

FIG. 6. Band alignment (with respect to a common vacuum level) of (a) monolayers GaS and GaSe and (b) monolayers GaSe and InS, considering three cases: (i) the monolayers keep their own lattice constant (left panel), (ii) both monolayers assume an average lattice constant (middle panel), and (iii) the monolayer with the smaller lattice constant is stretched to the larger lattice constant in the heterostructure (right panel). For cases (ii) and (iii) we also show the band-edge positions of the heterostructures. The lattice constants of the monolayers (in Å) are indicated in parentheses at the bottom of the figures. All VBM and CBM values are in eV.

the trends in the CBM and VBM levels for different lattice constants are correctly captured in DFT-PBE calculations; in fact, as discussed in Sec. III A, the changes in the band gaps as a function of biaxial strain obtained in our PBE calculations are consistent with results obtained using the HSE06 hybrid functional reported in Refs. [7,26].

Finally, as discussed in Sec. III A, our DFT-PBE calculations show that biaxial strain has a strong effect on the band edges of monolayer MMCs, being more pronounced for the CBM level (as we can also see from the deformation potentials listed in Table I). Thus, assuming that both layers of a heterostructure have the same lattice constant can lead to a wrong estimation of the band gap, in particular for GaS/GaSe, which is expected to form an incommensurate heterostructure. In fact, for GaS/GaSe [Fig. 6(a)], considering that both GaS and GaSe have the lattice constant of GaSe, we found a band gap of 0.90 eV, which is ∼50% smaller than the band gap computed from the band alignment of the isolated layers with their equilibrium lattice constants. For the InS/GaSe heterostructure, which has a smaller mismatch and is closer to the commensurate case, the difference is smaller: the band gap of the heterostructure with the lattice constant of InS (3.90 Å) is 0.97 eV while the band gap computed from the band levels of the individual layers is 1.16 eV.

IV. CONCLUSIONS

In summary, our DFT calculations demonstrate the importance of strain for the band gap in group-III monochalcogenides and for the band alignment in heterostructures of these materials. Due to the sensitivity to strain, commensurate heterostructures (where at least one layer is strained) must be distinguished from those where each layer keeps its own lattice constant (termed incommensurate heterostructures in this study) when addressing their electronic properties. We devised a simple scheme that allows us to provide an estimate if a commensurate or an incommensurate heterostructure is energetically preferred. In the incommensurate case, an additional energy penalty accounting for the lack of proper registry between the layers must be considered in addition to the van der Waals attraction in the energy balance. To obtain this energy penalty, we explored the potential energy landscape of a series of configurations with different stacking. Specifically, we studied GaS/GaSe with a lattice mismatch of 4.7% and GaSe/InS with a lattice mismatch of 2.1%, but we stress that this approach is not specific to these systems and can be applied to any 2D/2D van der Waals heterostructure. For the commensurate case, we systematically investigated the effect of strain on the band gap and band-edge positions of the individual monolayers. We found, in particular, that the CBM is much more sensitive to strain than the VBM, with a deformation potential more than twice as large as the deformation potential of the VBM. For the GaS/GaSe heterostructure, the high sensitivity of the CBM makes the band alignment also very sensitive to strain, as a small variation (∼0.36%) in the lattice constant of GaS may lead to a transition from type-I to type-II alignment. Finally, by comparing the energy cost of straining the layers in the commensurate case with the cost due to the lack of proper registry between the layers in the incommensurate structures, we found that GaSe/InS is expected to form a commensurate system, while an incommensurate configuration is more favorable for the GaS/GaSe heterostructure.

ACKNOWLEDGMENTS

A.U.R. acknowledges the Higher Education Commission (HEC) of Pakistan through the International Research Support Initiative Program (IRSIP). J.M.M. and P.K. gratefully acknowledge the computing time granted by the Center for Computational Sciences and Simulation (CCSS) of the University of Duisburg-Essen and provided on the supercomputer magnitUDE (DFG Grants No. INST 20876/209-1 FUGG and No. INST 20876/243-1 FUGG) at the Zentrum für Informations- und Mediendienste (ZIM). G.R. acknowledges HEC of Pakistan for supporting this research under the project electronic structure calculations using density-functional theory.

[1] P. Hu, Z. Wen, L. Wang, P. Tan, and K. Xiao, ACS Nano **6**, 5988 (2012).

[2] S. R. Tamalampudi, Y.-Y. Lu, R. Kumar U., R. Sankar, C.-D. Liao, K. Moorthy B., C.-H. Cheng, F. C. Chou, and Y.-T. Chen, Nano Lett. **14**, 2800 (2014).

[3] H. Huang, P. Wang, Y. Gao, X. Wang, T. Lin, J. Wang, L. Liao, J. Sun, X. Meng, Z. Huang, X. Chen, and J. Chu, Appl. Phys. Lett. **107**, 143112 (2015).

[4] W. Feng, J.-B. Wu, X. Li, W. Zheng, X. Zhou, K. Xiao, W. Cao, B. Yang, J.-C. Idrobo, L. Basile, W. Tian, P. Tan, and P. Hu, J. Mater. Chem. C **3**, 7022 (2015).

[5] See Supplemental Material at http://link.aps.org/supplemental/10.1103/PhysRevMaterials.2.094002 for details on the geometric arrangement and structural parameters of monolayer and bilayer GaS, GaSe, InS, and InSe.

[6] P. Miro, M. Audiffred, and T. Heine, Chem. Soc. Rev. **43**, 6537 (2014).

[7] H. L. Zhuang and R. G. Hennig, Chem. Mater. **25**, 3232 (2013).

[8] S. Lei, X. Wang, B. Li, J. Kang, Y. He, A. George, L. Ge, Y. Gong, P. Dong, Z. Jin, G. Brunetto, W. Chen, Z.-T. Lin, R. Baines, D. S. G. Ao, J. Lou, E. Barrera, K. Banerjee, R. Vajtai, and P. Ajayan, Nat. Nanotechnol. **11**, 465 (2016).

[9] D. T. Do, S. D. Mahanti, and C. W. Lai, Sci. Rep. **5**, 17044 (2015).

[10] Y. Ma, Y. Dai, M. Guo, L. Yu, and B. Huang, Phys. Chem. Chem. Phys. **15**, 7098 (2013).

[11] G. Mudd, M. R. Molas, X. Chen, V. Zólyomi, K. Nogajewski, Z. R. Kudrynskyi, Z. D. Kovalyuk, G. Yusa, O. Makarovsky, L. Eaves, M. Potemski, V. I. Fal'ko, and A. Patanè, Sci. Rep. **6**, 39619 (2016).

[12] C. S. Jung, F. Shojaei, K. Park, J. Y. Oh, H. S. Im, D. M. Jang, J. Park, and H. S. Kang, ACS Nano **9**, 9585 (2015).

[13] C. R. Woods, L. Britnell, A. Eckmann, R. S. Ma, J. C. Lu, H. M. Guo, X. Lin, G. L. Yu, Y. Cao, R. V. Gorbachev, A. V. Kretinin, J. Park, L. A. Ponomarenko, M. I. Katsnelson, Y. N. Gornostyrev, K. Watanabe, T. Taniguchi, C. Casiraghi, H.-J. Gao, A. K. Geim, and K. S. Novoselov, Nat. Phys. **10**, 451 (2014).

[14] W. Kohn and L. J. Sham, Phys. Rev. **140**, A1133 (1965).

[15] P. Giannozzi, S. Baroni, N. Bonini, M. Calandra, R. Car, C. Cavazzoni, D. Ceresoli, G. L. Chiarotti, M. Cococcioni, I. Dabo, A. D. Corso, S. de Gironcoli, S. Fabris, G. Fratesi, R. Gebauer, U. Gerstmann, C. Gougoussis, A. Kokalj, M. Lazzeri, L. Martin-Samos, N. Marzari, F. Mauri, R. Mazzarello, S. Paolini, A. Pasquarello, L. Paulatto, C. Sbraccia, S. Scandolo, G. Sclauzero, A. P. Seitsonen, A. Smogunov, P. Umari, and R. M. Wentzcovitch, J. Phys.: Condens. Matter **21**, 395502 (2009).

[16] J. P. Perdew, K. Burke, and M. Ernzerhof, Phys. Rev. Lett. **77**, 3865 (1996).

[17] A. Tkatchenko and M. Scheffler, Phys. Rev. Lett. **102**, 073005 (2009).

[18] N. Troullier and J. L. Martins, Phys. Rev. B **43**, 1993 (1991).

[19] H. J. Monkhorst and J. D. Pack, Phys. Rev. B **13**, 5188 (1976).

[20] L. Bengtsson, Phys. Rev. B **59**, 12301 (1999).

[21] V. Zólyomi, N. D. Drummond, and V. I. Fal'ko, Phys. Rev. B **87**, 195403 (2013).

[22] S. Demirci, N. Avazlı, E. Durgun, and S. Cahangirov, Phys. Rev. B **95**, 115409 (2017).

[23] H. Sun, Z. Wang, and Y. Wang, AIP Adv. **7**, 095120 (2017).

[24] M. Yagmurcukardes, R. T. Senger, F. M. Peeters, and H. Sahin, Phys. Rev. B **94**, 245407 (2016).

[25] T. Hu, J. Zhou, and J. Dong, Phys. Chem. Chem. Phys. **19**, 21722 (2017).

[26] H. Jin, J. Li, Y. Dai, and Y. Wei, Phys. Chem. Chem. Phys. **19**, 4855 (2017).

[27] J. Jalilian and M. Safari, Phys. Lett. A **381**, 1313 (2017).

[28] Y. Sun, S. Luo, X.-G. Zhao, K. Biswas, S.-L. Li, and L. Zhang, Nanoscale **10**, 7991 (2018).

[29] L. Hu, X. Huang, and D. Wei, Phys. Chem. Chem. Phys. **19**, 11131 (2017).

[30] W. Ibarra-Hernández, H. Elsayed, A. H. Romero, A. Bautista-Hernández, D. Olguín, and A. Cantarero, Phys. Rev. B **96**, 035201 (2017).

[31] J. He, K. Hummer, and C. Franchini, Phys. Rev. B **89**, 075409 (2014).

[32] J. Kang, J. Li, S.-S. Li, J.-B. Xia, and L.-W. Wang, Nano Lett. **13**, 5485 (2013).

[33] W. Wei, Y. Dai, C. Niu, X. Li, Y. Ma, and B. Huang, J. Mater. Chem. C **3**, 11548 (2015).